

## Permafrost degradation in the ice-wedge tundra terrace of Paulatuk Peninsula (Darnley Bay, Canada)

Rodrigue Tanguy<sup>a,\*</sup>, Dustin Whalen<sup>b</sup>, Gonçalo Prates<sup>a,c</sup>, Pedro Pina<sup>d</sup>, Pedro Freitas<sup>a,f</sup>, Helena Bergstedt<sup>e</sup>, Gonçalo Vieira<sup>a,f</sup>

<sup>a</sup> Centre of Geographical Studies, TERRA Associated Laboratory, Institute of Geography and Spatial Planning, University of Lisbon, Lisbon, Portugal

<sup>b</sup> Natural Resources Canada, Dartmouth, Canada

<sup>c</sup> Superior Institute of Engineering, University of Algarve, Faro, Portugal

<sup>d</sup> Institute of Astrophysics and Space Sciences, Department of Earth Sciences, University of Coimbra, Coimbra, Portugal

<sup>e</sup> b.geos, Korneuburg, Austria

<sup>f</sup> Centre of Northern Studies, University Laval, Quebec, Canada

### ARTICLE INFO

#### Keywords:

Permafrost degradation  
Ice-wedge polygons  
Marine submersion  
Infrastructures

### ABSTRACT

The warming of high latitudes climate is enhancing the degradation of ground-ice and inducing important landscape changes across the Arctic. This new Arctic state affects geomorphological dynamics, hydrology, and ecosystems, and poses challenges to the stability of infrastructure and livelihoods of Arctic communities. This study focuses on the hamlet of Paulatuk within the Inuvialuit Settlement Region of the Amundsen Gulf, south Darnley Bay, in northern Canada. In the summer of 2019, an ultra-high resolution aerial survey with a fixed-wing Unmanned Aerial Vehicle (UAV) was conducted, generating a 5 cm spatial resolution orthomosaic and Digital Surface Model (DSM). These, together with field observations were used to produce a very-high resolution geomorphological map of the settlement and surrounding coastal areas. Landscape changes were analyzed using historical aerial imagery of 1975 and 1993, the 2019 UAV survey and a very-high resolution Pléiades satellite scene from 2020. The area is a tundra terrace made up of sandy fluvioglacial sediments affected by a dense network of ice-wedge polygons, mostly high-centered, but also low-centered, showing signs of permafrost degradation. Air and ground temperatures have increased respectively by 0.8 and 1.9 °C over last two decades at Paulatuk, and inter-polygon ponds surface increased by 23,000 m<sup>2</sup> since 1975 due to ice-wedge thawing. The airstrip enhanced thaw pond formation on its margins, especially after 1993. The DSM reveals a depression south of the airstrip, which can be potentially flooded due to its proximity to the coastal waters.

### 1. Introduction

Recent warming of the Arctic region is causing a change in the thermal regime of permafrost and is leading to a reduction of its extent (Biskaborn et al., 2019; Li et al., 2022; Smith et al., 2022). The general temperature increase of permafrost results in its progressive degradation and thawing, observed by the thickening of the active layer in several regions of the northern hemisphere (Li et al., 2022). In this context, thermokarst processes are enhanced, leading to widespread changes in permafrost landscapes (Jones et al., 2019). Thermokarst is a term widely used to refer to the processes and landforms associated with thawing ground-ice and ground surface collapsing, shaping typical permafrost landscapes (Dylik and Ryzczynska, 1964; Kokelj and Jorgenson, 2013).

Permafrost warming leads to an increase in ground-surface instability, such as erosion, subsidence, or mass movements, resulting in the geomorphological change of typical permafrost landforms and the generation of thermokarst landforms such as thaw slumps, thermokarst lakes and ponds (Lantuit and Pollard, 2008; Grosse et al., 2013; Andresen and Loughheed, 2015; Radosavljevic et al., 2016; Karjalainen et al., 2020). The exacerbated development of thermokarst landforms has potential impacts on terrestrial and aquatic ecosystems due to the consequent transport of sediments and organic carbon during flow of material along retrogressive thaw slumps (Lantuit and Pollard, 2008; Kokelj and Jorgenson, 2013; Jones et al., 2018) or with sudden thaw lake drainage (Jones et al., 2022). In addition, accelerated permafrost degradation is an emerging issue for Arctic societies and infrastructure

\* Corresponding author.

E-mail address: [rodrigue.tanguy@edu.ulisboa.pt](mailto:rodrigue.tanguy@edu.ulisboa.pt) (R. Tanguy).

<https://doi.org/10.1016/j.geomorph.2023.108754>

Received 21 January 2023; Received in revised form 24 May 2023; Accepted 24 May 2023

Available online 29 May 2023

0169-555X/© 2023 The Author(s). Published by Elsevier B.V. This is an open access article under the CC BY license (<http://creativecommons.org/licenses/by/4.0/>).

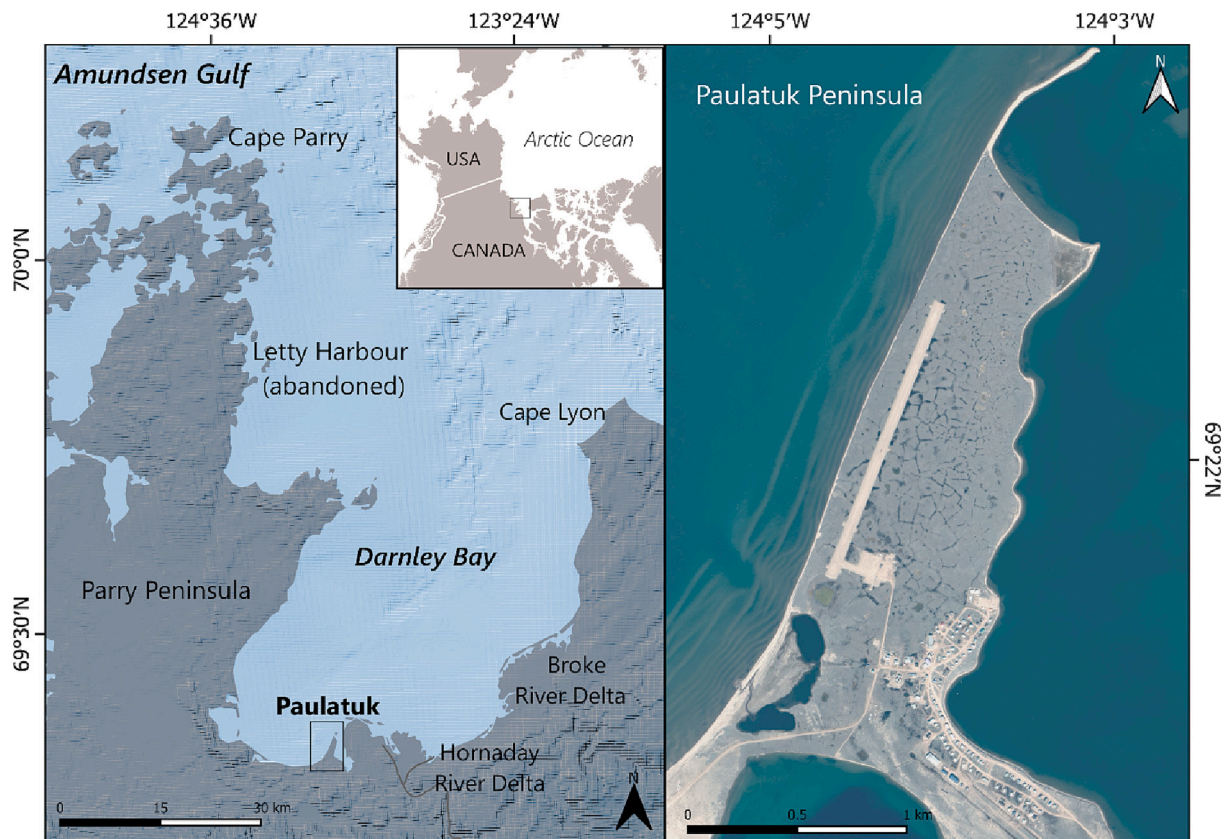


Fig. 1. Location of Paulatuk Peninsula. Basemap: GSHHG, GEBCO and PLEIADES © CNES, 2020, distribution Airbus DS. Projection: WGS 84/UTM zone 10.

stability, posing new challenges in civil engineering (Hjort et al., 2022; Liew et al., 2022). There is a need to better identify signs of permafrost degradation, in order to inform and promote adaptation policies in concerned communities (Irrgang et al., 2019; Larsen et al., 2021). A common landform widely distributed in lowland permafrost terrain are ice-wedge polygons formed by the infiltration of melt water into surficial winter contraction ground-cracks, which then freezes and pushes the soil laterally, growing by the succession of cracking and freezing cycles (Black, 1976; MacKay, 2002; Fritz et al., 2016; Kanevskiy et al., 2017; Frappier and Lacelle, 2021). Ice-wedge polygons can be classified into several types, namely low-center, flat-center, and high-center polygons, which define the polygon shape, based on the stage of formation and the degree of ice-wedge degradation. The flat-centered polygons are characteristic of the initial phase of ice-wedge formation where their growth has not yet significantly transformed the topography. Low-centered polygons develop as ice wedge growth displaces sediments laterally and form raised rims at the margin of the ice wedge with a trough down the middle. The center of the polygon is lower, and often presents water ponding. When ice-wedges have undergone a thermokarst phase, their thawing results in the inversion of the topography to high-centered polygon shape where inter-polygon ponds occupy troughs. This form is specific to ice-wedge degradation (MacKay, 2002; Kanevskiy et al., 2017, 2022). Ice-wedge degradation has increased in recent decades, leading to environmental changes and infrastructures stability problems (Raynolds et al., 2014; Fritz et al., 2016; Liljedahl et al., 2016; Nitzbon et al., 2019). When exposed on the coast, on high cliffs, ice-wedges promote mass wasting through block failure due to ground ice-thawing and cliff foot scouring by waves during summer (Hoque and Pollard, 2016). Thermokarst lakes and water retention ponds are also signs of ice-rich permafrost degradation and result from ground-ice thawing, surface subsidence and water retention (Fritz et al., 2016). Initially these features form by the merging of thaw ponds located above ice-wedge troughs (i.e., inter-polygon ponds), by

low-centered polygon ponds or by the subsidence of a thawing ice-rich ground filled by water. However, permafrost degradation can lead to drainage of these water bodies caused by the degradation of ice-wedge troughs adjacent to the lake margins, creating gullies, eventually discharging into coastal waters (Grosse et al., 2013; Fritz et al., 2016; Nitzbon et al., 2019; Kartoziia, 2019). Water in ponds and lakes can seep out due to thickening of the active layer, or by thaw progression during the warm season (Andresen and Lougheed, 2015). Ground surface subsidence is another factor associated with permafrost degradation. Inter-annual subsidence movements are related to active layer thickness variations, precipitation, and water infiltration. This phenomenon is an issue for infrastructure and could significantly impact Arctic communities. For instance, in Nunavik, northern Canada, permafrost degradation is affecting airfields and roads, posing engineering challenges (Oldenborger and LeBlanc, 2015; Allard et al., 2020; Gruber, 2020). Already, some coastal settlements, such as Shishmaref (Alaska) and Tuktoyaktuk (Canada), threatened by erosion and marine submersion, are requiring relocation works and plans to adapt to climate change (Radosavljevic et al., 2016; Whalen et al., 2022).

This study focuses on the Inuvialuit settlement of Paulatuk, south of Darnley Bay, northern Canada, and aims to investigate recent landscape changes, assessing permafrost degradation from 1975 to 2020. Shoreline change assessment has been established at Paulatuk, revealing significant recent bluff-top retreat due to thermo-denudation and waves attack, especially along the western coast showing retreat rates up to 0.8 m/yr. Erosion has doubled in recent decades in response to recent warming, longer ice-free season and increasing storminess (Sankar et al., 2019; Tanguy et al., 2023). However, little is known about the geomorphology, environmental conditions and landform changes occurring inland in the interior of the peninsula, where human presence has increased since the 1970's. Historical aerial images and very-high resolution satellite imagery were used to investigate these landscape changes. An ultra-high resolution Unmanned Aerial Vehicle (UAV)

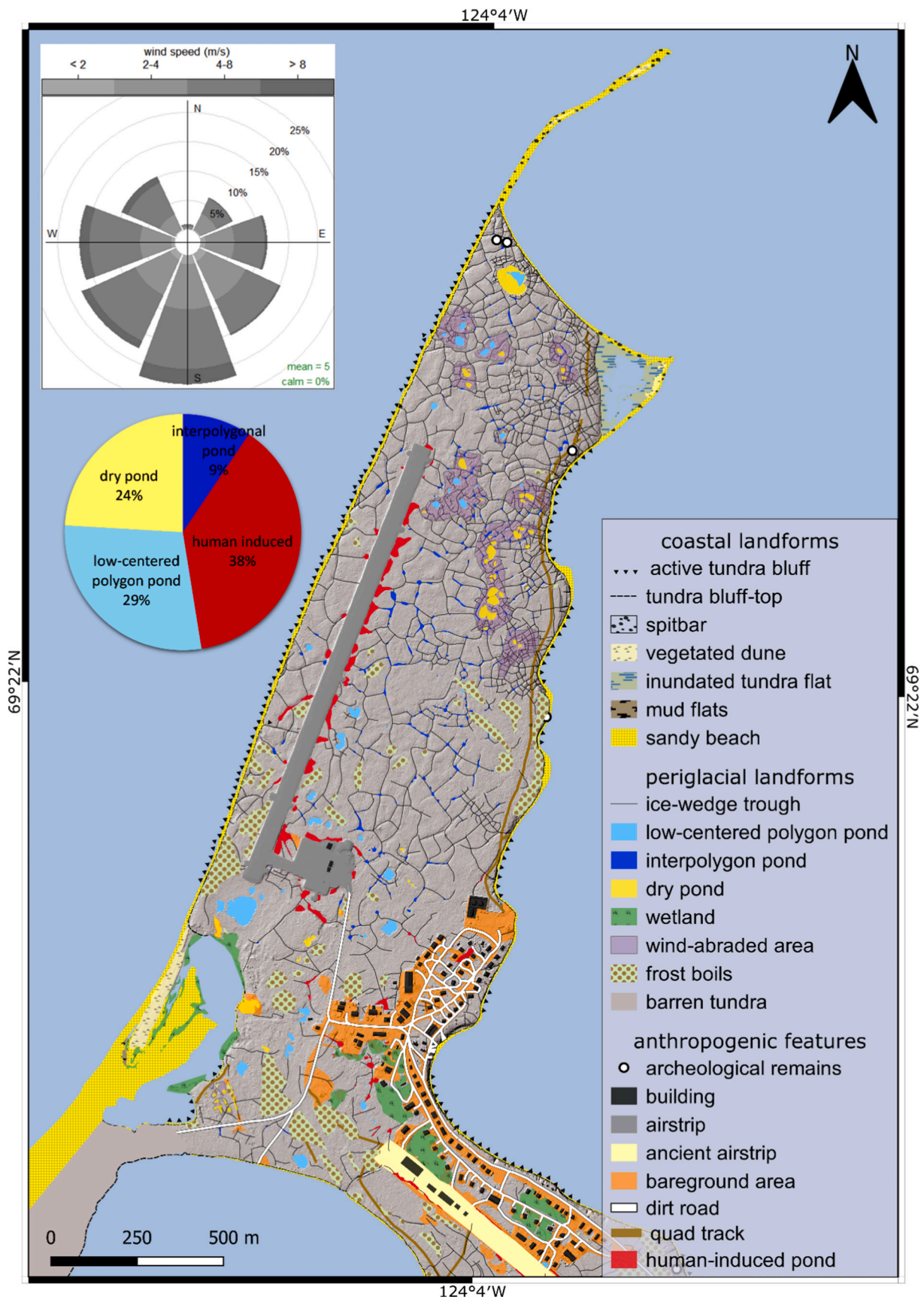


Fig. 2. High resolution geomorphological map of Paulatuk Peninsula in 2019. The base layer is the hillshade derived from the UAV survey. The pie-chart included represents the area fraction of the different thaw ponds. The wind rose was created with data downloaded from NASA, n.d. (<https://power.larc.nasa.gov/data-access-viewer/>).

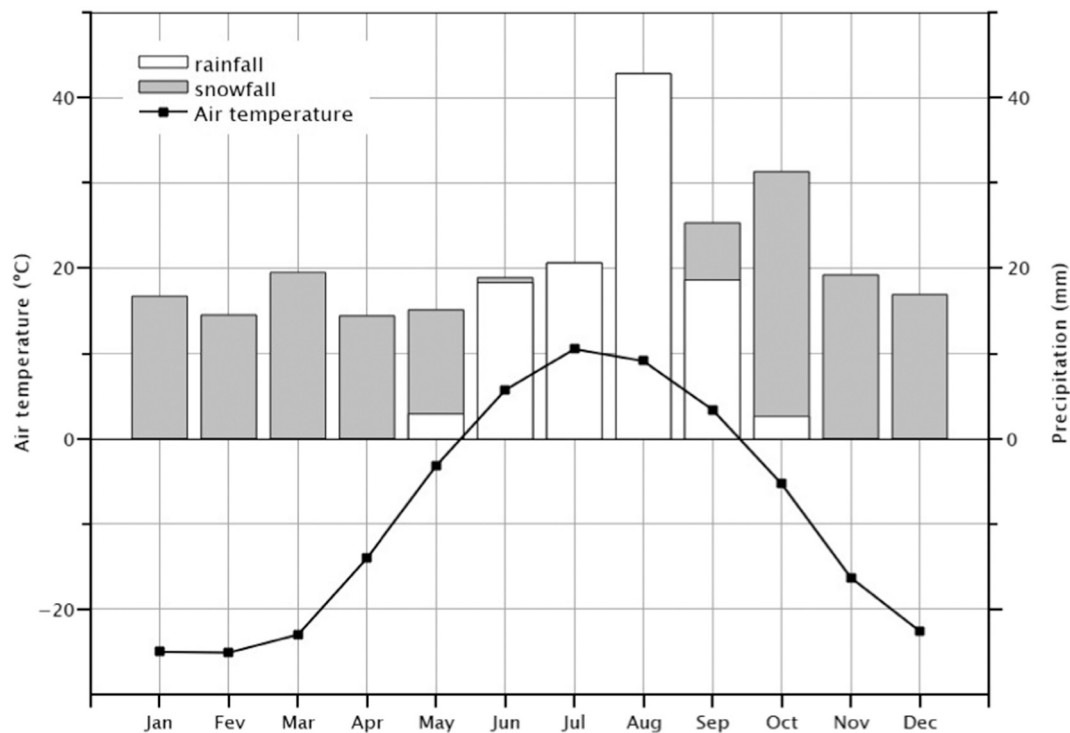


Fig. 3. Climograph of Paulatuk. Data recorded at the Paulatuk weather station, downloaded via climatedata.ca (1988–2020, [ECCC, 2023](https://climatedata.ca)).

survey-derived digital surface model and orthomosaic were used to generate a detailed geomorphological map of the settlement at an unprecedented scale. This paper analyses the geomorphology of Paulatuk Peninsula and highlights the potential flooding risk associated with sea-level rise and subsidence, as well as the effects of infrastructure on the degradation of ice-wedges and the potential positive feedback on permafrost degradation generated by water impoundment.

## 2. Regional setting

### 2.1. Geography

The Darnley Bay region is in the continuous permafrost zone and consists of Paleozoic carbonate bedrock to the northwest and Mesozoic sandstones and Pleistocene moraine deposits to the south and east (Yorath et al., 1975; Kerr, 1994). The peninsula of Paulatuk is situated on the southern coast of Darnley Bay, northern Canada (69° 21' N, 124° 04' W) and is ca. 3.5 km long and 0.9 km wide, extending in a SSW-NNE direction (Fig. 1). It presents a flat terrace surface with altitudes up to 6 m, limited by low bluffs. The terrain is formed by morainal deposits of late Wisconsin silts and sands that outcrop on the shoreline (Evans et al., 2021), and the terrace presents widespread ice-wedge polygon networks. The coast is affected by a microtidal regime with a range from 0.3 to 0.5 m (Kerr, 1996). Prevailing winds, as well as the strongest winds (>15 m/s) are from the south-southwest (Fig. 2), with ventifacts formed by southerly katabatic winds (Mackay and Burn, 2005). The western coast shows a low active tundra bluff 3 m high, with a straight profile, fronted by a narrow sandy beach around 10 m wide (see Appendix A), exposed to a maximum fetch of 77 km to the north and 11 km to the west (Fig. 1). This coast is subject to the highest erosion rates, with up to 0.8 m/yr from 1993 to 2020 (Tanguy et al., 2023). A sandy spit anchored at the northern tip of the peninsula stretches north-eastwards for about 680 m, showing the effects of longshore drift mobilizing sediments from southwest to northeast.

The eastern coast is stable, facing a maximum fetch of approximately 2.3 km to the northeast and shows a low tundra bluff and a narrow sandy

beach with four small embayments associated with erosion-deposition dynamics. Longshore drift moves sediments from the south to north, as revealed by the depositional forms at the concave sections. The barrier island system located 3.6 km to the north associated to the Hornaday River Delta, provides sheltered conditions to the eastern side of Paulatuk, making it an ideal emplacement for docks and fishing vessels (see Appendix B). On the southwest, an enclosed coastal lagoon of 70,000 m<sup>2</sup> seems to be the result of the breaching of two ancient thermokarst lake basins submerged by coastal waters (Fig. 1). This lagoon is partially enclosed by a ridged beach system and overwash fans that show evidence of flooding events, which may occur during spring tides coupled with storm swells and surges. The northeast sector of the peninsula is an inundated tundra flat under tidal influence, partially enclosed by two narrow barrier beaches also subject to overwash events (see Appendix A). The interior of the peninsula is characterized by ice-wedge polygons and different types of thaw ponds. The highest surfaces show scarce vegetation, evidencing wind desiccation and nivo-aolian corrasion (Fig. 2). Extensive areas with frost boils occur along the coast and around vegetation denuded and bare patches areas (see Appendix B). The settlement is only accessible by air or sea and the original airstrip that was built south of the hamlet was rebuilt along the peninsula, close to the west coast, in 1991. In 2022, Paulatuk accounted for 327 inhabitants (GNWT, 2022), with housing located along the southeastern coast of the peninsula, at a higher ground level between 3 and 5 m (Fig. 2). The current airstrip is located close to the west coast of Paulatuk Peninsula. It is 1.3 km long and 55 m wide, with a mean altitude of 4.2 m, artificially installed over a ~2 m thick gravel pad overlying the tundra and numerous ice-wedge troughs (see Appendix B). Water retention on its boundaries is evident, as well as in the ancient airstrip and within the hamlet, where infrastructure and land-use limit the drainage (see Appendices A and B).

### 2.2. Climatic and environmental conditions

Paulatuk shows a dry-cold climate, with the hottest month (July), presenting a mean air temperature of 8.7 °C and the coldest month

**Table 1**  
Remote sensing and derived data used in this study.

Data	Acquisition period	Number of scenes	Scale	Bands	Pixel size (m)	Mean RMSE (m)
Aerial photography (black and white)	Aug 1975	1	1:25000	1	0.6	1.6
	Aug 1993	3	1:5000	1	0.6	1.3
UAV orthomosaic	Aug 2019	1	–	1	0.05	–
UAV DSM	Aug 2019	1	–	1	0.05	–
Pléiades (multispectral, pansharpened)	Aug 2020	1	–	4	0.5	0.35
Permafrost-cci active layer thickness/ground temperatures	2000–2020	–	–	1	1000	–

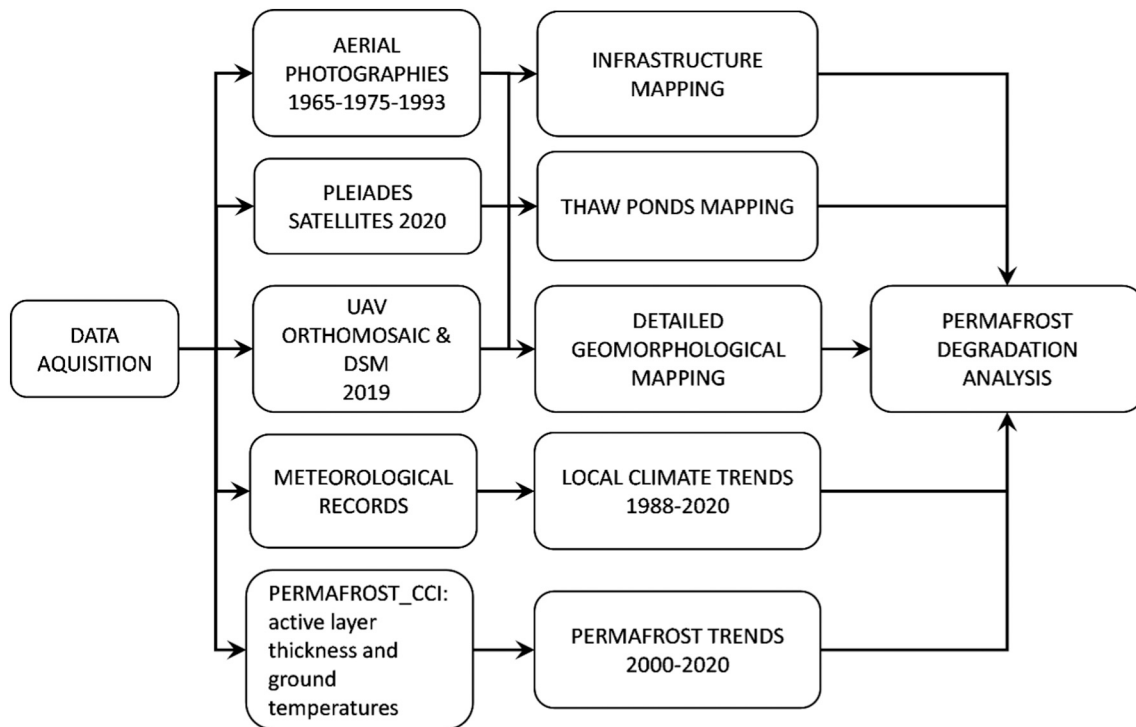


**Fig. 4.** Detailed workflow of image and data analysis.

(February), showing  $-25.1$  °C (Fig. 3). Extreme temperatures ranged from  $-46.9$  to  $+30.3$  °C from 1988 to 2020 (ECCC, 2023). Paulatuk receives annually a total amount of rain of 106 mm concentrated between July and October and a total annual amount of snow of 145 mm from October to May (ECCC, 2023). Based on the ice charts of the Canadian Sea Ice Service, in the Darnley Bay area, the sea-ice break-up starts around the 2nd of July and freeze-up ends around the 22nd of October. Significant open-water conditions (sea-ice concentration  $< 10$  %), lasted for around 12 weeks, from the 16th of July to the 8th of October for the period 1981–2010 (ECCC, 2011). From 1965 to 2016, summer sea-ice decreased by 11 to 15 % per decade within the Amundsen Gulf mouth region (Derksen et al., 2019), and the open-water season is estimated to increase by 0.2 weeks per year due to delayed freeze-up in the Darnley Bay area (Galley et al., 2016). Storm frequency and open-water temperatures have been increasing in the region since 1970, impacting shoreline dynamics in the area (Atkinson, 2005; Sankar et al., 2019). Relative sea level is expected to rise between 80 and 120 cm at the mouth of the Amundsen Gulf by 2100 and by 106 cm at Paulatuk according to the high-emissions scenario RCP8.5 (James et al., 2021). Mean annual ground temperatures from  $-5$  to  $-10$  °C, have been recorded at Paulatuk from a 28 m deep borehole between 2008 and 2009 and the results provided evidence of permafrost warming during that period (Smith et al., 2010).

### 3. Materials and methods

#### 3.1. General framework

This work combines the use of ultra-high-resolution UAV imagery from 2019, historical monochrome aerial imagery from 1975 and 1993, and very-high resolution satellite imagery acquired in 2020 (Table 1).

The historical aerial imagery has been orthorectified and georeferenced in ENVI 5.6 through Rational Polynomial Coefficient (RPCs) and Ground Control Points (GCPs) attribution with the Pléiades 2020 satellite imagery which were used as ground-truth data. The detailed geomorphological mapping of the Paulatuk Peninsula and settlement was done using the ultra-high resolution 2019 UAV orthomosaic and Digital Surface Model (DSM). To investigate permafrost degradation, thaw ponds, buildings, and infrastructure were manually digitized using the 1975 and 1993 aerial imagery, the 2019 UAV orthomosaic, and the Pléiades 2020 image. The time-series analysis of meteorological records from the Paulatuk weather station was obtained from climatedata.ca. This dataset contains air temperature precipitation and snow-on-ground measurements for 1988–2020. Since current in-situ monitored permafrost temperatures and active layer thickness records are not available at Paulatuk, permafrost temperatures and active layer thickness trends were estimated using the satellite derived datasets from MODIS LST and ERA5, produced as part of the European Space Agency's (ESA) Climate Change Initiative (CCI) Permafrost project (Obu et al., 2021a, 2021b) (Fig. 4).

**Table 2**  
Legend of the geomorphological map of Paulatuk. Orthomosaic views are represented in [Appendix A](#).

	Feature	Definition
Coastal landforms	Tundra bluff top/ active tundra bluff	Unlithified cliffs composed of frozen poorly consolidated material, such as organic matter, sand, silt, and clay. These cliffs are fronted by sandy and gravel narrow beaches and are sensitive to temperature changes and wave action presenting various erosional features.
	Inundated tundra flat	Very shallow submerged areas stretching until the foreshore zone. They are usually influenced by tides and present intertidal flats.
	Vegetated dunes	Present on top of accretional sandy stretches, formed by wind action coupled with sediment supply from currents and waves. Their stability is assessed by vegetation colonization.
	Sandy spit	Elongated sandy accumulations formed by the action of waves and associated littoral drift. It is anchored at the coast at its base and can enclose coastal lagoons.
	Mud tidal flats	Previously submerged mud flats along the ridged beaches enclosing coastal lagoons.
	Sandy beach	Narrow sandy accumulations along the cliffs subject to current and wave reworking.
	Periglacial features	Ice-wedge troughs
Inter-polygon pond		Water bodies formed by snow thawing and from ice-wedge degradation located on top of the ice-wedges troughs.
Low-centered polygon pond		Shallow water bodies formed by the melting of ground-ice and snow in centered depressions formed by ice-wedge polygons.
Dry pond		Drained thaw ponds due infiltration following thaw progression, by gullyng or by evaporation.
Wetland		Poorly drained wet soils composed of sediments and organic material.
Wind abraded area		Areas denuded of vegetation, which are generally convex and above the terrace, resulting in wind abrasion and desiccation, with salt extrusion.
Frost boils		Type of patterned ground, forming mud circles due to cryoturbation activity.
Anthropogenic features	Barren Land	Low vegetation of small shrubs, grasses and mosses adapted to typical of tundra terrains.
	Archeological remains	Stone structures from the Thule/Copper traditions (1200 CE to 1500). Now vegetated, they have a circular or rectangular shape. These structures were used as tent/winter house rings or to conserve food.
	Transport infrastructures Buildings	Airstrip and gravel roads. Buildings and other construction sites such as docks and fuel reservoirs.
	Disturbed areas	Bare-ground patches identified associated to human activity generally for construction purposes or quad tracks.

**Table 2 (continued)**

Feature	Definition
Human-induced Pond	Large thaw ponds are localized in the margins of infrastructures such as the airstrips and around buildings due to the water retention. They are often associated with ice-wedge thawing, especially along the actual airstrip.

### 3.2. UAV imagery

A UAV survey of the Paulatuk Peninsula and hamlet was carried out in July–August 2019 providing a 3D base survey and ground truthing data for satellite imagery analysis. The imagery was collected using a Sense Fly eBee Classic fixed-wing UAV with a Sensefly SODA 20 MP optical camera, collecting aerial photos with a ground sampling resolution of 5 cm. Georeferencing was done using a Trimble R4 system with a base and a rover surveying in RTK DGPS mode. The base position was obtained by post-processing using the NRCAN PPP Service. The survey consisted of 58 Ground Control Points (GCPs) distributed over the 3.4 km<sup>2</sup> survey area to georeference the point cloud. Processing of the images was done using PIX4D mapper to generate the point cloud, orthomosaic and DSM. The root mean square error (RMSE) of the point cloud calculated using 17 independent check points was 0.04 m (X), 0.03 m (Y) and 0.08 m (Z). The ultra-high resolution of the orthomosaic and the DSM allowed for the identification and highly accurate mapping of the landforms and infrastructure.

### 3.3. Very-high resolution satellite imagery

Pléiades (CNES) satellite imagery acquired over the region in 2020 was ordered from ISIS Airbus. The scene is a pansharpened multispectral image with a spatial resolution of 0.5 m corrected using rational polynomial coefficients (RPCs) in ENVI 5.6. The real color composite enabled the identification of geomorphological features and water flooding areas, including small ponds, and their digitizing with high accuracy. This scene was the base for historical aerial imagery orthorectification and co-registration. The high accuracy of the image allowed for identification of detailed ground control points (polygon intersections, lake features and infrastructure) that were consistent between the images.

### 3.4. Detailed geomorphological mapping

The ultra-high-resolution UAV orthomosaic and the DSM allowed the production of a very detailed geomorphological map ([Fig. 2](#)). The legend has been constructed regarding the different physical processes and anthropogenic activities present in the area ([Table 2](#)). The coastal landforms were identified by their link to meteo-marine forcings inducing erosion, accretion, or flooding. The periglacial landforms were identified as those resulting from terrestrial processes governed by thermokarst, such as ice-wedge troughs and thaw. Anthropogenic features referring to transport infrastructure, such as dirt roads and airstrips, buildings, and disturbed areas (e.g., bare-ground surfaces) associated with human activity ponds (see [Appendices A and B](#)).

## 4. Results

### 4.1. Climate and permafrost change

The meteorological data from the Paulatuk station shows an increase in mean air temperatures of 0.4 °C per decade from 1988 to 2020 and 0.8 °C per decade from 2000 to 2020. The annual precipitation increased by 40 mm per decade from 1988 to 2020 but decreased by 27 mm per decade in the last two decades. Individual records for rain and snowfall

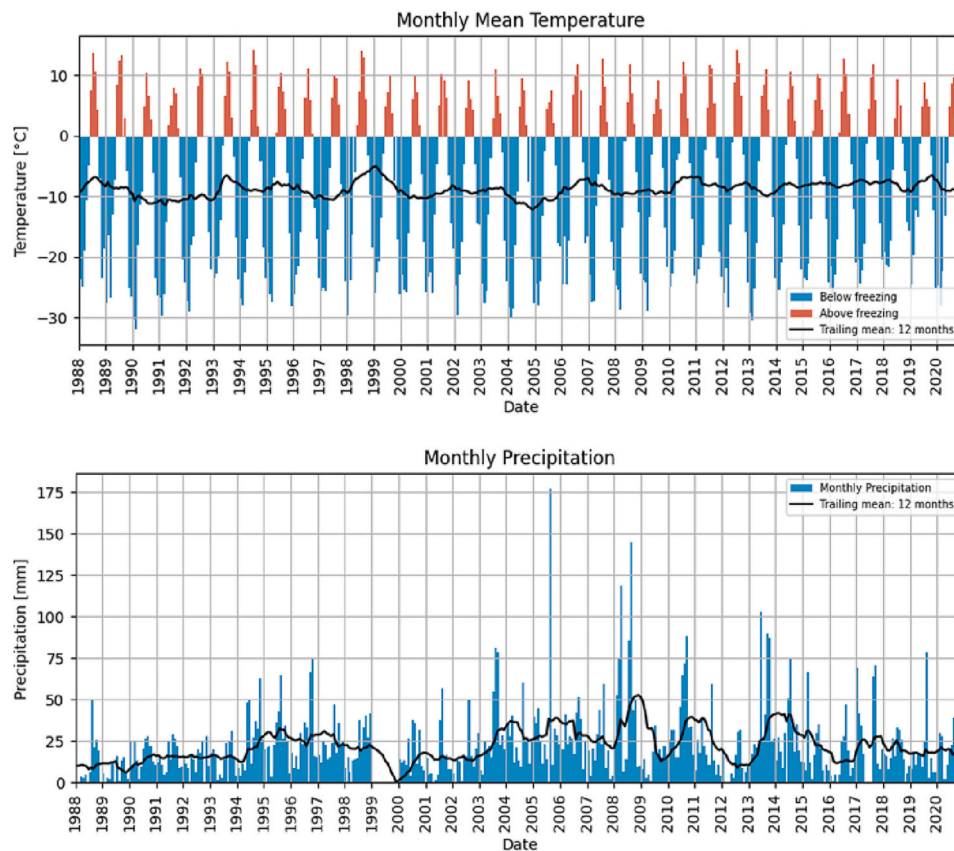


Fig. 5. Air temperatures and precipitations time-series at Paulatuk station over the period 1988–2020. Dataset acquired via climatedata.ca and plots created with noaaplotter (Nitze, 2023).

Table 3

Decadal trends for meteorological and permafrost variables at Paulatuk from 1988 to 2020 (climate dataset from climatedata.ca and permafrost model data from Obu et al., 2021a, 2021b).

Environmental variable	Decadal trend		
	1988–2020	1988–2014	2000–2020
Air temperature (°C)	+0.4	–	+0.8
Total precipitation (mm)	+40	–	–27
Rainfall (mm)	–	+25	–
Snowfall (mm)	–	+27	–
Snow-on-ground (cm)	–2	–	–3
Active layer thickness (m)	–	–	+0.1
Ground temperature (°C)	–	–	+1.3

are only available for 1988 to 2014, during which the amounts increased respectively from 25 to 27 mm per decade. Snow cover has decreased by 3 cm per decade during the recent. The summers of 1998, 2006 and 2012 were very hot with temperatures up to 3 °C above average. The years 2005, 2008, 2010 and 2013 recorded a very-high amount of precipitation, with up to three times more than average (Fig. 5).

Active layer thickness and ground temperature time-series modelled from satellite data from 2000 to 2020 (Obu et al., 2021a, 2021b) show a thickening of the active layer of 0.1 m per decade and an increase in ground temperatures of 1.3 °C per decade 2000–2020 (Table 3).

#### 4.2. Ice-wedge polygon network

Ice-wedge troughs sum up to 6.2 km in length and are mostly concentrated north of the settlement limit. The ice-wedge density map (Fig. 6a) represents the number of ice wedges present in a radius of 100 m and shows that polygons are more concentrated in the northeast of the

peninsula, being the result of the subdivision of the principal ice-wedges into secondary or tertiary ice-wedges. The dense areas (>10 ice-wedge troughs/100 m radius) show a higher mean altitude at 3.8 m when compared to the rest of the peninsula lying at a mean altitude of 3.4 m (Figs. 2, 6b), exposing them to wind corrosion, resulting in bare vegetation surfaces. We note that the densely fractured areas form a microtopography with elevated soil rims, dry ponds, and deep ice-wedge troughs, resulting in an irregular surface relief. The major ice-wedge subdivision of these areas suggest that ice-wedge formation has been occurring earlier, where ponds have had time to develop, merge and drain. A difference in the sedimentary materials could explain this ice-wedges troughs density. The rest of the peninsula is characterized by a more regular ice-wedge polygon pattern with less subdivision, revealing a younger ice-wedges network. These areas are characterized by flat-centered and low-centered polygon types. Along the coast is found a larger presence of high-centered polygons. This form reveals an advanced phase in ice-wedge degradation where the polygon center shows higher altitude compared to degraded ice-wedge troughs.

#### 4.3. Changing permafrost

##### 4.3.1. Subsidence

The DSM reveals a low-lying area south of the airstrip where there is a gradual southward decrease in elevation, linking into a large thaw pond, suggesting the occurrence subsidence (Figs. 6b and 7). This thermokarst depression shows an average diameter of 180 m and an area of 27,000 m<sup>2</sup> below 1 m a.s.l. The airstrip slopes towards the depression with a maximum angle of 0.37°, suggesting that subsidence is occurring and affecting the airstrip (Fig. 7). The depression is separated from the adjacent pond to the south by a rim about 0.5 m high and 70 m wide, sensitive to breaching or submersion (Fig. 7; profile 1). Westwards, the

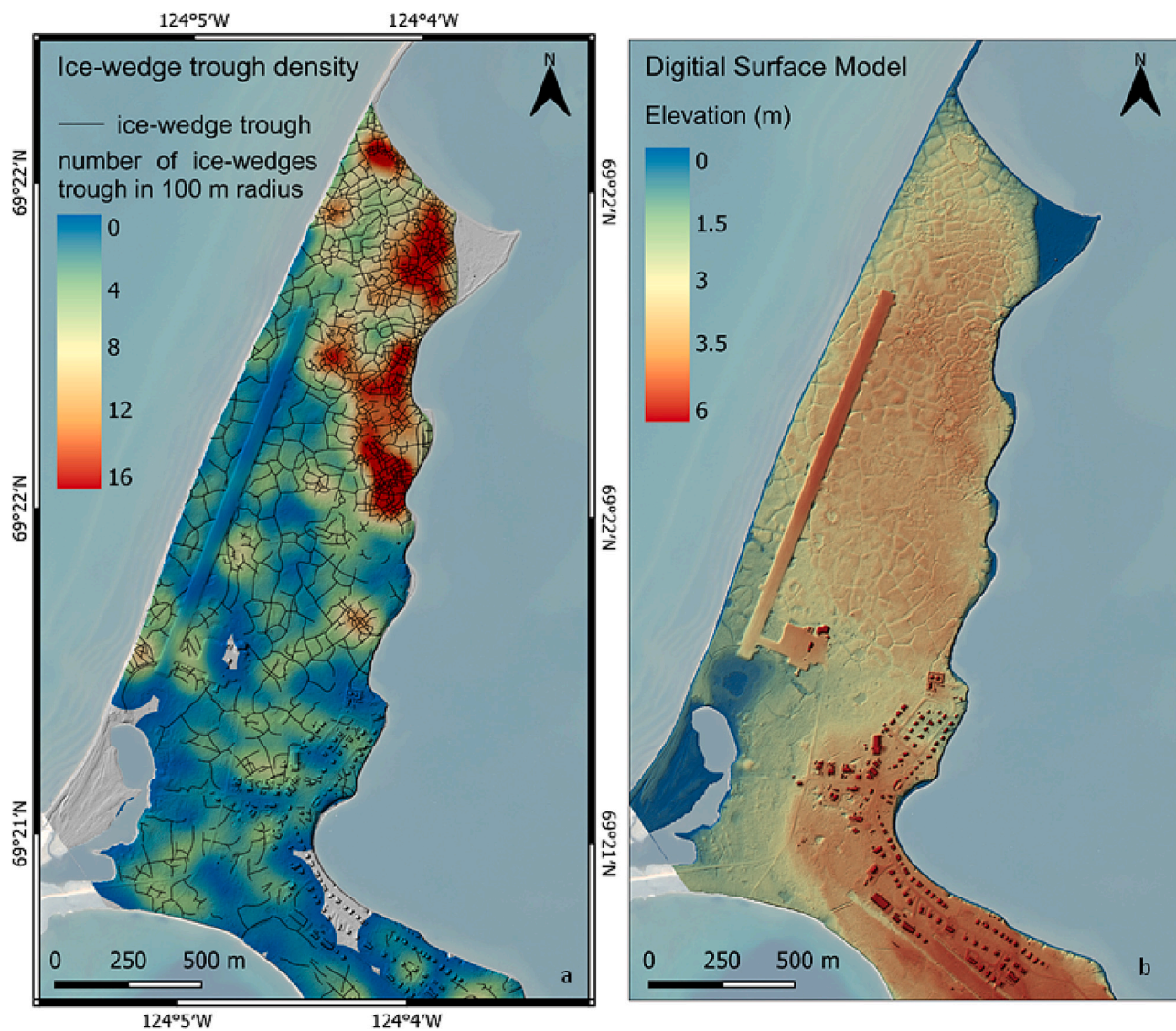


Fig. 6. Density map of ice-wedge troughs (a), the legend represents the presence of ice-wedges in radius of 100 m around their center. Digital Elevation Model with hillshading in Paulatuk (b). Basemap: PLEIADES © CNES, 2020, distribution Airbus DS. Projection: WGS 84/UTM zone 10.

depression center (highlighted by the intersection of profiles 1 and 2) is separated from the open ocean by an interfluvial that is <2 m in height (Fig. 7; profile 2). Flooding of the depression by coastal waters associated with storm surge events or sea level rise could further induce erosion and subsidence, exposing the airstrip to increasing hazard. Relative sea level is expected to rise by 80 to 120 cm by 2100 at the mouth of the Amundsen Gulf, and by 106 cm at Paulatuk (James et al., 2021).

Fig. 8 illustrates the areas potentially floodable areas following sea level rise of 80 and 120 cm. For both scenarios, the submerged zones are the northern spit, the inundated tundra area in the northeast, and the ridged beaches and the depression mentioned above, in the southwest. Note that the submergence of the southern beach system would result in the direct exposure of the lagoon's backshore to coastal waters. In addition, the large lake located directly south of the peninsula, could be affected by salinization. However, note that in this specific area, coastal dynamics are characterized by stable-accreting beaches during recent decades and erosion is not yet a major problem.

#### 4.3.2. Thaw pond evolution since 1975

The analysis of the UAV orthomosaic of 2019 allowed to map 692 thaw ponds, covering a total area of 80,000 m<sup>2</sup> and classified into

different types: i. low-centered polygon ponds, where polygon boundaries are elevated due to recent formation or expansion of the ice-wedges, ii. inter-polygon ponds, resulting from ice-wedge thawing and subsidence in the troughs forming elongated shape, iii. merged inter-polygonal, generally at ice-wedge intersections and showing irregular shapes (see Appendix A). The low-centered polygon ponds occupy the largest total area, but inter-polygon ponds have a larger number, although with smaller area and occupying deeper depressions in the troughs. Several dry ponds are also present, occurring mainly in dense ice-wedge areas and are often adjacent to ice-wedges troughs. Some dry ponds show a clay floor with desiccation cracks, while others show grass colonization (see Appendix A and Fig. 12). Several large ponds are located along the ancient and current airstrip, which may result of enhanced ice-wedge degradation promoted by the presence of infrastructures, having been classified as human-induced ponds for the analysis.

The results show a significant increase in the pond number and area induced by the development of buildings and infrastructure since 1975 (Figs. 10 and 11), expanding at an average rate of 9.2 m<sup>2</sup>/year with a total increase of 18,000 m<sup>2</sup> between 1975 and 2020. The inter-polygon ponds increased at a rate of 8 m<sup>2</sup>/year, with a total increase of 23,000 m<sup>2</sup>. Low-centered polygon pond surface did not show a clear trend with

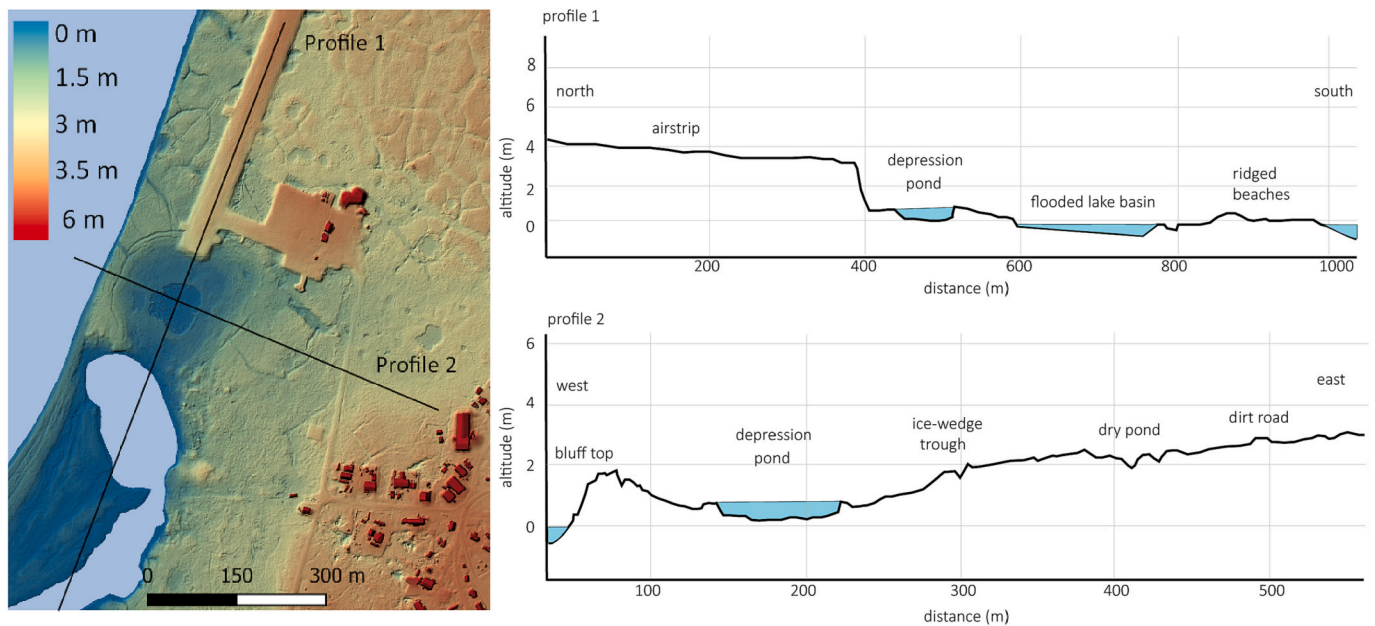


Fig. 7. Digital surface model of the south of Paulatuk Peninsula with cross-sections showing the topography and subsidence occurring in the south sector of the airstrip.

the area decreasing between 1975 and 1993 (Fig. 9). However, the image from 1975 may show an overestimated low-centered polygon pond surface due to the aerial photo contrast and resolution influencing the definition of dry areas of small water bodies. The increasing observations of inter-polygonal ponds support the theory of permafrost degradation during that time-period (Fig. 12). The snow accumulation along the airstrip embankment may also contribute to increased water availability in summer and to a reduction in ground cooling in winter, promoting permafrost warming and degradation (Allard et al., 2020).

#### 4.4. Anthropogenic impacts

The human impact on the landscape was assessed by a landscape change analysis between 1975 and 2020 (Table 4; Figs. 10, 11). In 1975, the settlement counted 24 elevated houses and one airstrip at the southeast of the peninsula. The progressive increase of the population, reaching 327 inhabitants in 2022, has been accompanied by terrain artificialization. A new airstrip was constructed in 1991, while the older one was located at the south of the hamlet. By 2020, there were 124 buildings on the peninsula, a new and larger airstrip, a network of dirt roads, and extensive bare-ground areas. Since 1975, the number of buildings has multiplied by 5.1 and their area has been multiplied by 9.3 (Table 4). Bare-ground areas represent 190,000 m<sup>2</sup> in 2020, mostly located around the settlement and being the result of material removal or deposition for construction purposes such as dirt roads, building basements or ponds infilling. As shown above, this alteration of natural permafrost terrain has been accompanied by a significant development of thaw ponds (Figs. 10 and 11). Human-induced ponds developed from underlying ice-wedge thawing and from the accumulation of thaw water of original inter-polygonal ponds along infrastructure, particularly the airstrips. In 1975, human-induced ponds were only present along the older airstrip. Since then, their number has been multiplied by 14.5 and their area by 2.1 (Table 4). New inter-polygonal ponds have developed, and their surface area has increased by a factor of 12 since 1975. On the contrary, low-centered polygon situation remains generally stable in time.

Figs. 10 and 11 show thaw pond development along the eastern side of the airstrip infill and close to the buildings. The airstrip was identified as a major driver for the enlargement of thaw ponds due to water

drainage inhibition. Aerial photographs from 1993 show that ponds had just developed, especially around the airstrip and still showed an early stage of degradation (Fig. 10). On the contrary, the low-centered polygon ponds are older and were already present in 1975.

## 5. Discussion

### 5.1. Ice-wedge polygon network

The geomorphological mapping of ice-wedge troughs revealed that the northwest of the Paulatuk Peninsula presents a denser polygon network due to more frequent secondary and tertiary ice-wedge subdivisions (Fig. 6). Ice-wedge formation and distribution patterns are complex. Their subdivision is related to the age and genetic difference between soil material types, soil moisture, ground-ice concentration, soil moisture as well as winter climate variations. Low-order fractures forms during warm winters and high order fissures during cold winters (Burn and O'Neill, 2015). As observed around low-centered polygons, frequent ice-wedge cracking is much more favorable in ridged polygons than in high-center polygons (Abolt et al., 2018). Dense ice-wedge areas may also suggest that different stratigraphic units outcropped in Paulatuk Peninsula (Oliva et al., 2014) show a higher clay content, explaining their greater susceptibility to cracking. Studies have shown that ice-wedge polygon microtopography controls tundra hydrology, snow depth, and ice-wedge thermal regime (Liljedahl et al., 2016; Wainwright et al., 2017; Abolt et al., 2018). Rims of raised soil in the polygon periphery have the effect of increasing snow depth in low-lying areas promoting water storage and ponding. However, the degradation of the polygon microtopography, trough ice-wedge thawing or rim collapse, can also profoundly affect the hydrology by causing a rapid drainage of the surrounding thaw ponds through gullying and seepage (Liljedahl et al., 2016). These observations could explain the presence of drained thaw ponds in areas with significant fractures.

### 5.2. Permafrost degradation

The dynamics of thaw pond formation is a good indicator of permafrost degradation. The increasing surficial water in inter-polygon ponds indicates ice-wedge degradation and that soil artificialization

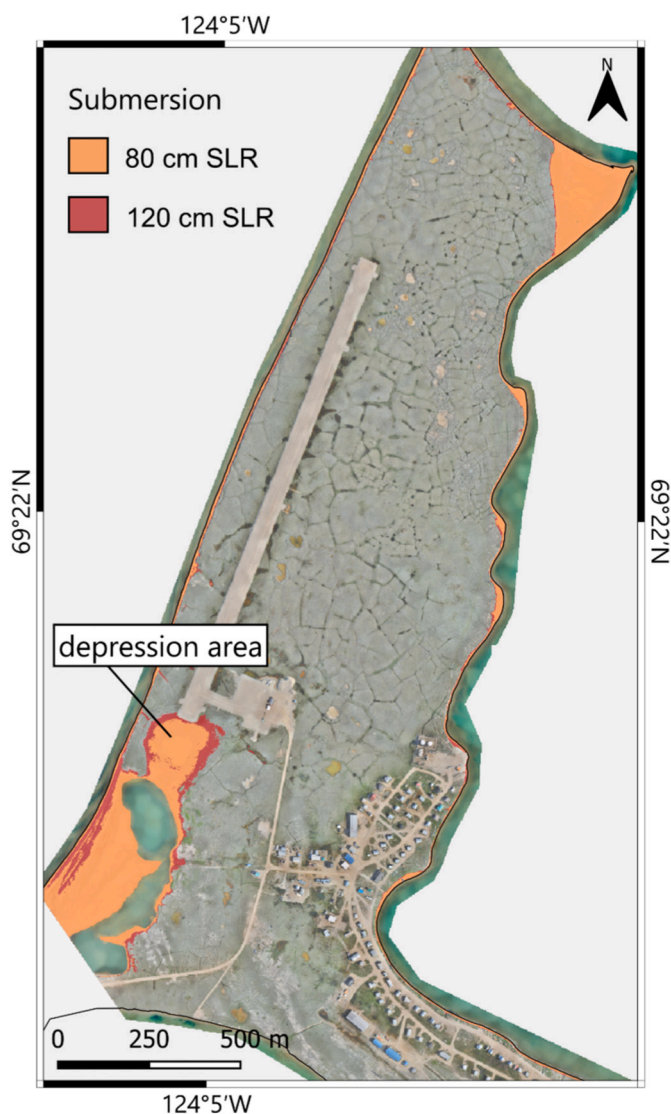


Fig. 8. Potential floodable area from relative sea level rise of 80 to 120 cm by 2100. Basemap: UAV orthomosaic, 2019.

enhanced impoundments. The analysis of historical images allowed for the identification of a significant increase of thaw ponds, particularly along the airstrip embankments right after its construction in 1991 (Fig. 10). However, the degradation can also be triggered by interannual climatic variations. The summers of 1998, 2006 and 2012 were particularly warm in Paulatuk, with average temperatures above 9 °C with a general warming trend in air and ground temperatures over the last decades. However, the inter-annual variability in the dynamics of thaw pond surfaces may be large and vary during the thaw season. Thawing, evaporation, infiltration, and seasonal variability remain difficult to quantify and their timing response needs to be considered for accurate analysis. For example, the presence of dry ponds suggests that some have disappeared due to a variety of factors, including evaporation, vegetation growth, or sedimentary infill and/or drainage. Pond water may also drain through thickening of the active layer or during the warm season by simple thaw progression and infiltration (Andresen and Loughheed, 2015). Climate models forecast a shift in Arctic hydroclimatology to a rain-dominated era in the Arctic by 2050–2080, strongly linked to Arctic warming and declining sea ice (Bintanja and Selten, 2014; Box et al., 2019). Warmer and wetter conditions in the Arctic will lead to a decrease in terrestrial snow cover, affect soil moisture, and exacerbate permafrost thaw, but will also impact wildlife and indigenous communities (McCrystall et al., 2021). Under these conditions, Paulatuk Peninsula may face significant permafrost degradation issues.

### 5.3. Increasing anthropogenic impacts

These results highlight that the presence of infrastructure seems to

Table 4  
Evolution of thaw ponds and infrastructure in Paulatuk between 1975 and 2020.

Pond type	1975		2020	
	n° of ponds	Area (×10 <sup>3</sup> m <sup>2</sup> )	n° of ponds	Area (×10 <sup>3</sup> m <sup>2</sup> )
Human-induced	6	17	87	36
Inter-polygonal	94	2	331	26
Low-centered	64	33	36	21
Total	164	52	454	83
Infrastructures	n°	Area (×10 <sup>3</sup> m <sup>2</sup> )	n°	Area (×10 <sup>3</sup> m <sup>2</sup> )
Buildings	24	3	124	28
Airstrip	1	57	1	100

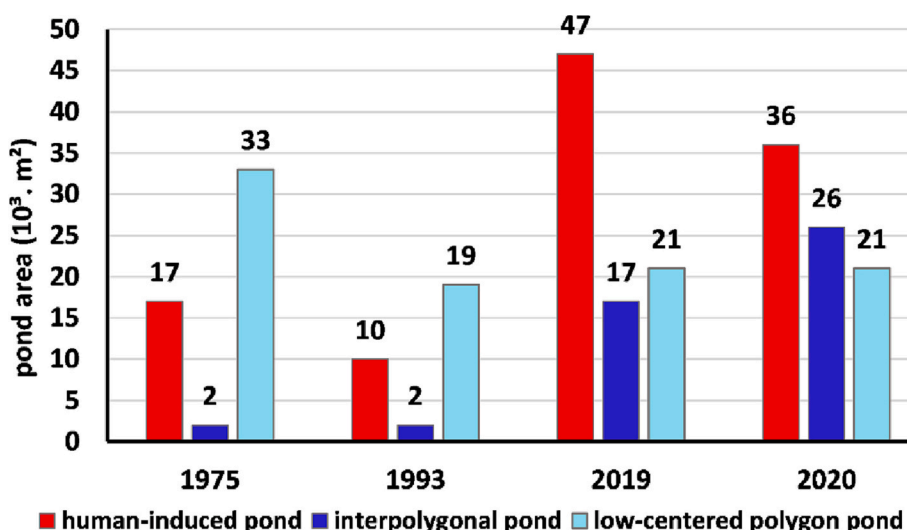
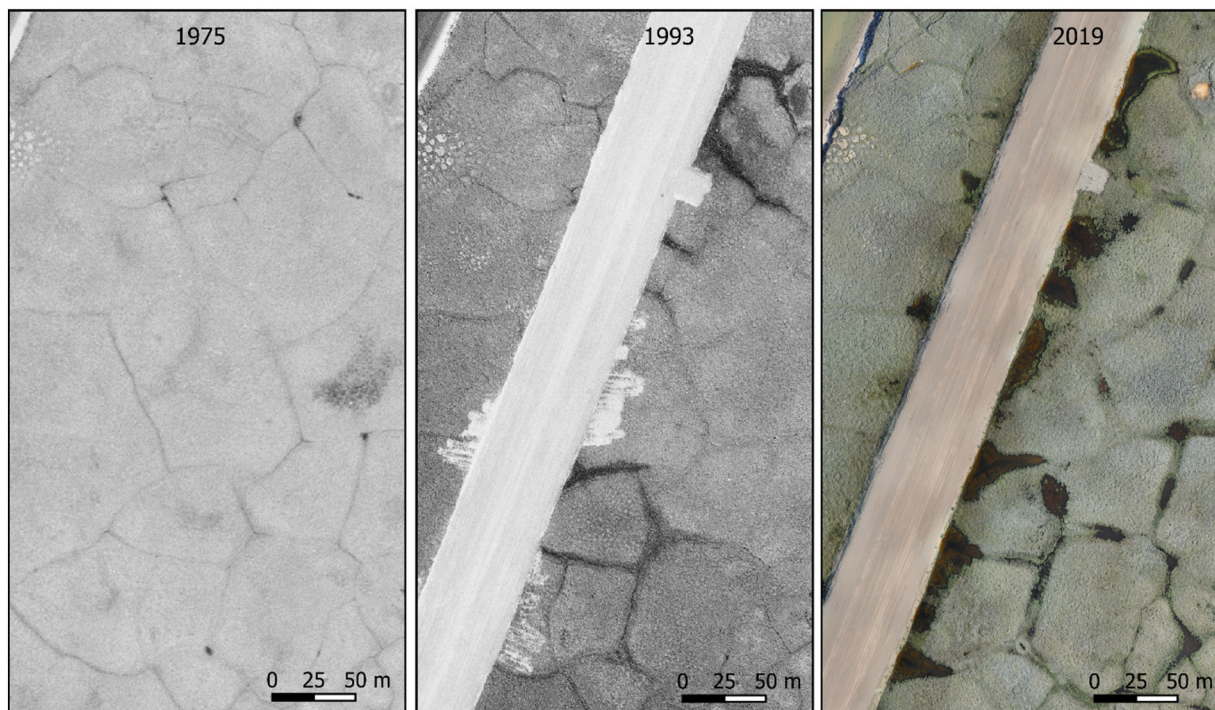


Fig. 9. Thaw pond surface evolution between 1975 and 2019.



**Fig. 10.** Thaw pond formation along the airstrip between 1975, 1993 and 2019. (Imagery: NRCAN 1975, 1993; UAV orthomosaic 2019).

significantly influence the evolution of recent thaw ponds, leading to the degradation of permafrost and pond expansion (Figs. 10, 11). The airstrip embankment seems to be showing a thermal effect on the ground, with detailed topography suggesting subsidence in the south part of the strip. However, no data exists on subsidence for the area. As occurred in other hamlets in the north, snow may accumulate at the side of the airstrip embankment contact, leading to a larger volume of water during summer, enhancing thaw pond formation. Similar observations have been made at the Tasiujaq airstrip in Quebec (Allard et al., 2012). There, the snow cover was thicker along the embankment foot due to the dominant winds, acting as an isolator and preventing the cooling of the ground surface. Snow accumulation and poor water drainage result in water retention along the runways. Thaw pond water retains heat from solar radiation and participates in downward heat diffusion inducing permafrost degradation and subsidence (Allard et al., 2020). Once the degradation has begun, the new soil surface conditions reinforce the degradation phenomena. However, research at the Prudhoe Bay Oilfield has shown that the degradation of ice wedges is a reversible process. Indeed, after a phase of partial degradation of the ice wedge, the lacustrine sedimentation of an intermediate layer protects the ice-wedge from further thawing. Hence, ice-wedge stabilization can occur despite the accumulation of snow and water in depressions and lead to the formation of new ice-wedges within the newly sedimented layers. These processes were also observed in areas with infrastructure (Kanevskiy et al., 2017, 2022), but the impact of warming may impede stabilization.

## 6. Conclusions

This study provides a detailed geomorphological map of the Paulatuk Peninsula, complemented with the analysis of the geomorphic and hydrological indicators of permafrost degradation since 1975. The main conclusions are:

1. The detailed geomorphological map produced with the 2019 UAV orthoimage and DSM allowed for a better understanding of the terrestrial and coastal processes affecting the peninsula and associated landforms. Ice-wedges are a predominant feature associated

with thawing processes inducing pond development. The spatial distribution of ice-wedge, more concentrated in the northwest, suggests that these areas are composed of different cryostratigraphic units more prone to cracking

2. Over the last two decades, the average air and ground temperature have increased respectively by 0.08 and 0.13 °C per year, while total precipitation and snow cover have decreased.
3. Landforms associated to permafrost degradation linked to human activity have increased significantly. Since 1975, the human-induced ponds surface area has doubled, developing along the actual airstrip and within the settlement after 1993. The analysis of the thaw pond surface evolution between 1975 and 2020 suggests that ice-wedges are degrading faster in recent decades, leading to a widening of inter-polygon ponds, which have multiplied by 12 since 1975. The current airstrip plays a major role in the formation of thaw ponds along its margins. Being more concentrated along its eastward side, we speculate that the accumulation of snow on its margins enhances the development of thaw ponds.
4. The analysis of the DSM suggests that subsidence is affecting the southwest sector of the airstrip. This area could soon be particularly vulnerable to marine submersion.

This study shows that very high-resolution analysis using field observations and remote sensing data is an important approach for understanding the sensitivity of permafrost landscapes to human activity and to the recent warming of the Arctic. Indeed, coastal retreat rates have increased since the 1990's, as well as terrain degradation, rising challenges in terms of engineering. Inuit communities are on the front line of these consequences, which force modifications to the traditional ways of life. Adaptation measures and a holistic approach linking traditional to scientific knowledge is urgent to better plan and ensure food access, a healthy living, a sustainable economy, and a socio-ecological conditions adapted to the new Arctic.

## Declaration of competing interest

The authors declare that they have no known competing financial

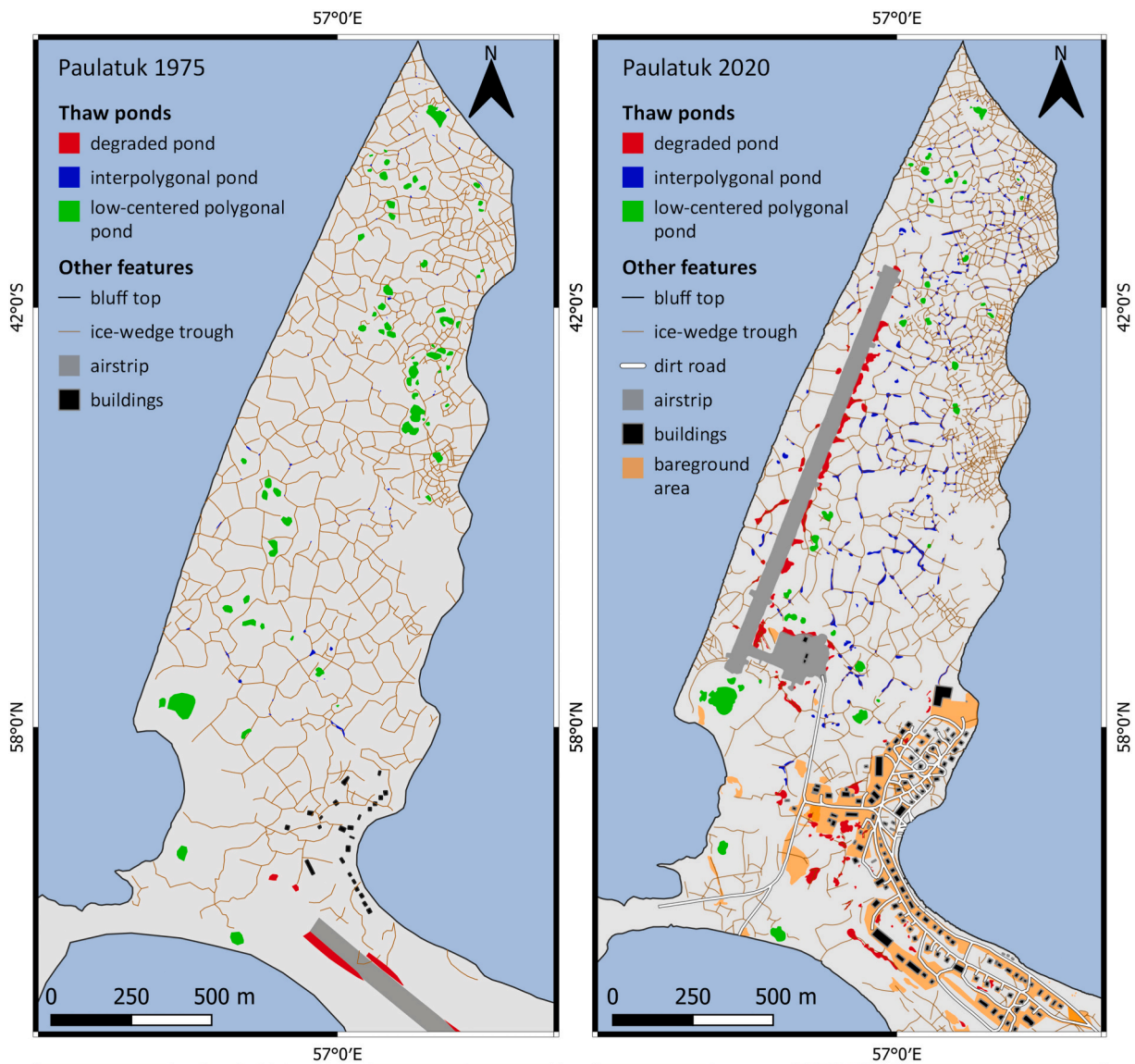


Fig. 11. Landscapes change between 1975 and 2019 in Paulatuk Peninsula. The shoreline represents the blufftop.

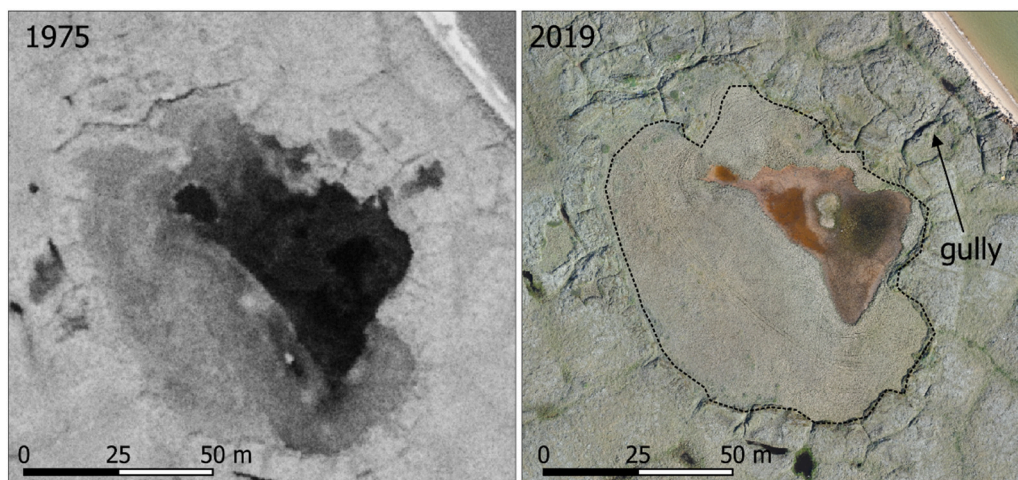


Fig. 12. Pond drainage from 1975 and 2019, showing vegetation colonization. Original extension of pond shown with a dotted line. The brown area shows the extent of the moist/saturated zone in the recent summers (UAV orthomosaic, 2019). (For interpretation of the references to color in this figure legend, the reader is referred to the web version of this article.)

interests or personal relationships that could have appeared to influence the work reported in this paper.

#### **Data availability**

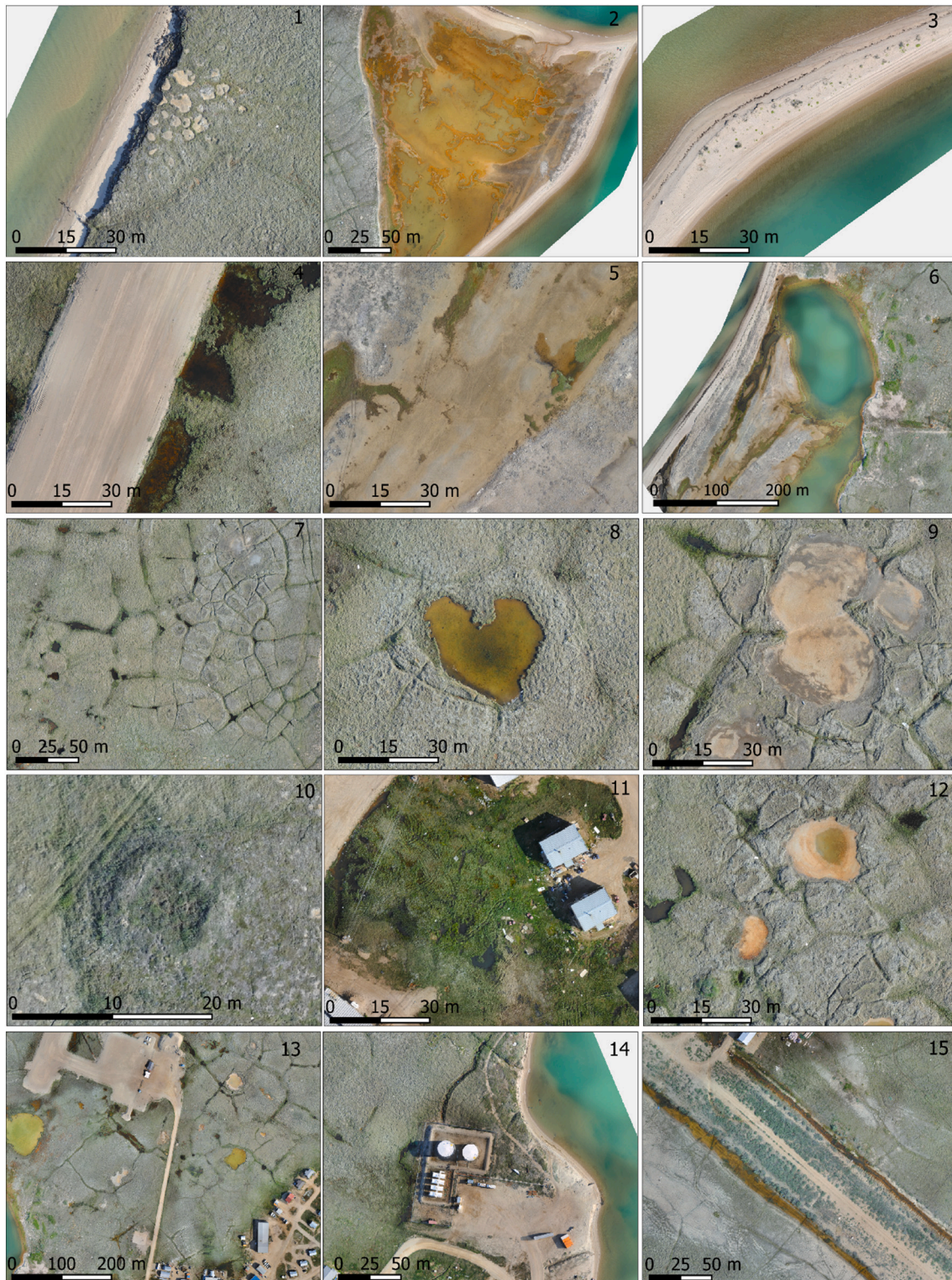
Data will be made available on request.

#### **Acknowledgements**

This work is part of the Nunataryuk project and was funded by the European Union's Horizon 2020 Research and Innovation Program under grant agreement no 773421 and supported by Natural Resources Canada, Climate Change Geoscience Program, Crown-Indigenous Relations, and Northern Affairs Canada (CIRNAC) through the Beaufort

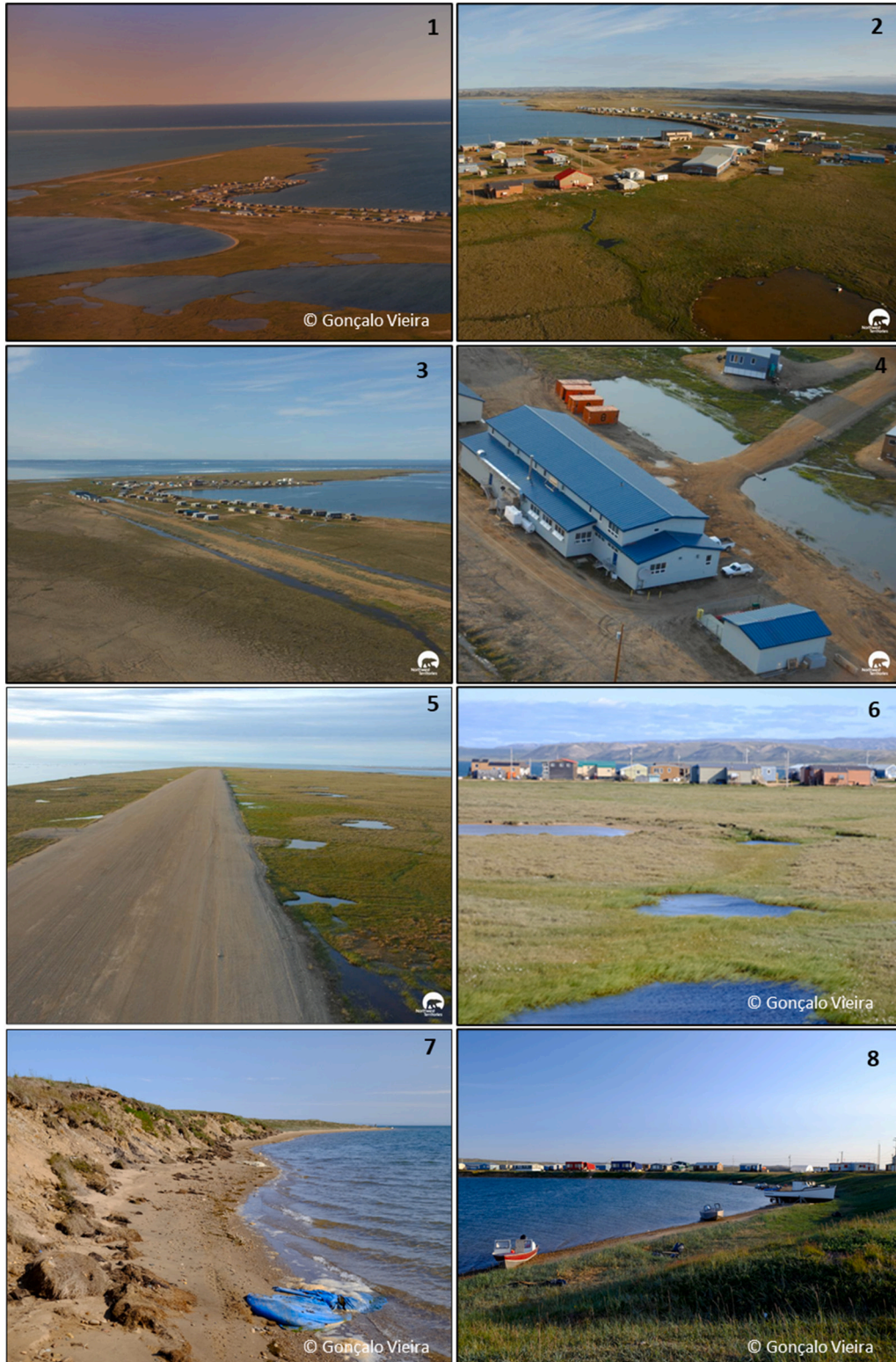
Sea Regional Strategic Environment and Research Assessment (BRSEA). This work was further supported by the European Commission, Horizon 2020 Framework Programme (CHARTER project grant no 869471) and European Research Council project no 951288 (Q-Arctic). Pleiades imagery was acquired through the ISIS Pléiades Program in connection with the WMO Polar Space Task Group. This work falls under the Northwest Territories Scientific Research permit (#16490), and support from the community of Paulatuk via consultation with the Hunters and Trappers committee in August 2019 and again in March 2020. Their advice and questions provided the basis of the research study. We thank the two anonymous reviewers for their comments that lead to significant modifications to the original manuscript and that contributed to improving the final version of the manuscript.

#### **Appendix A**



Views of the 2019 UAV orthomosaic used to build the geomorphological map legend with (Table 2). Active coastal bluff with froist boils (1), inundated low-tundra flat (2), sandy spit with vegetated dunes (3), human-induced pond along airstrip (4), mud flats (5), southern coastal lagoon enclosed by ridged beaches (6), ice-wedge polygons network (7), low-centered polygon pond (8), dry ponds (9), archaeological remains (10), wetlands (11), wind-abraded area (12), airstrip, dirt road and habitations (13), fuel reservoirs and bare-ground area (14), ancient airstrip and adjacent ponds (15).

Appendix B



Diverse aerial and ground terrain views of Paulatuk. Aerial photo of the peninsula (1), ice-wedge troughs and low-center polygonal pond (2), human-induced ponds along houses, ancient and actual airstrip (3, 4, 5), coastal bluff erosion along the inside coastline of the peninsula (7), sheltered coast (8). Source: Gonçalo Vieira; Government of Northwest Territories, 2009

## References

- Abolt, C.J., Young, M.H., Atchley, A.L., Harp, D.R., 2018. Microtopographic control on the ground thermal regime in ice wedge polygons. *Cryosphere* 12, 1957–1968. <https://doi.org/10.5194/tc-12-1957-2018>.
- Allard, M., Lemay, M., Barrette, C., L'Hérault, E., Sarrazin, D., Bell, T., Doré, G., 2012. Chapter 6: permafrost and climate change in Nunavik and Nunatsiavut: importance for municipal and transportation infrastructures. In: Allard, M., Lemay, M. (Eds.), *Nunavik and Nunatsiavut: From Science to Policy. An Integrated Regional Impact Study (IRIS) of Climate Change and Modernization*. ArcticNet Inc., Quebec City (QC), pp. 171–197.
- Allard, M., Chiasson, A., B. St-Amour, A., Mathon-Dufour, V., Aubé-Michaud, S., L'Hérault, E., Bilodeau, S., Deslauriers, C., 2020. Caractérisation géotechnique et cartographie améliorée du pergélisol dans les communautés nordiques du Nunavik. Rapport final. Centre d'études nordiques, Université Laval, Québec, p. 75.
- Andresen, C., Lougheed, V., 2015. Disappearing Arctic tundra ponds: Fine-scale analysis of surface hydrology in drained thaw lake basins over a 65-year period (1948–2013). *J. Geophys. Res. Biogeosci.* 120 (3), 466–479. <https://doi.org/10.1002/2014jg002778>.
- Atkinson, D.E., 2005. Observed storminess patterns and trends in the circum-Arctic coastal regime. *Geo-Mar. Lett.* 25, 98–109. <https://doi.org/10.1007/s00367-004-0191-0>.
- Bintanja, R., Selten, F.M., 2014. Future increases in Arctic precipitation linked to local evaporation and sea-ice retreat. *Nature* 509 (7501), 479–482. <https://doi.org/10.1038/nature13259>.
- Biskaborn, B.K., Smith, S.L., Noetzi, J., Matthes, H., Vieira, G., Streletskiy, D.A., Schoeneich, P., Romanovskiy, V.E., Lewkowicz, A.G., Abramov, A., Allard, M., 2019. Permafrost is warming at a global scale. *Nat. Commun.* 10 (1), 264. <https://doi.org/10.1038/s41467-018-08240-4>.
- Black, R.F., 1976. Periglacial features indicative of permafrost: ice and soil wedges. *Quat. Res.* 6 (1), 3–26. [https://doi.org/10.1016/0033-5894\(76\)90037-5](https://doi.org/10.1016/0033-5894(76)90037-5).
- Box, J.E., Colgan, W.T., Christensen, T.R., Schmidt, N.M., Lund, M., Parmentier, F.J.W., Brown, R., Bhatt, U.S., Euskirchen, E.S., Romanovskiy, V.E., Walsh, J.E., 2019. Key indicators of Arctic climate change: 1971–2017. *Environ. Res. Lett.* 14 (4), 045010. <https://doi.org/10.1088/1748-9326/aac1b>.
- Burn, C.R., O'Neill, H.B., 2015. Subdivision of ice-wedge polygons, Western Arctic Coast. In: *Proceedings of the 68th Canadian Geotechnical Conference and 7th Canadian Permafrost Conference, Canadian Geotechnical Society*, p. 66 (Richmond, BC).
- Derksen, C., Burgess, D., Duguay, C., Howell, S., Mudryk, L., Smith, S., Thackeray, C., Kirchner-Young, M., 2019. Changes in snow, ice, and permafrost across Canada. In: *Canada's Changing Climate Report*, vol. 5, pp. 194–260.
- Dylik, J., Rybczynska, E., 1964. Le thermokarst, phénomène négligé dans les études du Pléistocène. *Ann. Géogr.* 73 (399), 513–523. <https://www.jstor.org/stable/23445942>.
- Environment and Climate Change Canada, 2011. Canadian 30-year Ice Atlas 1981–2010. <https://iceweb1.cis.ec.gc.ca/30Atlas/page1.xhtml?grp=Guest&lang=en>. (Accessed 31 March 2023).
- Environment and Climate Change Canada & climatedata.ca, 2023. Historical climate data at Paulatuk station 1988–2020. <https://climatedata.ca/download/#station-download>. (Accessed 31 March 2023).
- Evans, D.J.A., Smith, I.R., Gosse, J.C., Galloway, J.M., 2021. Glacial landforms and sediments (landsystem) of the Smoking Hills area, NWT, Canada: implications for regional Pliocene-Pleistocene Laurentide Ice Sheet dynamics. *Quat. Sci. Rev.* 262. <https://doi.org/10.1016/j.quascirev.2021.106958>.
- Frappier, R., Lacelle, D., 2021. Distribution, morphology, and ice content of ice-wedge polygons in Tombstone Territorial Park, central Yukon, Canada. *Permafr. Periglac. Process.* 32 (4), 587–600. <https://doi.org/10.1002/pp.2123>.
- Fritz, M., Wolter, J., Rudaya, N., Palagushkina, O., Nazarova, L., Obu, J., Rethemeyer, J., Lantuit, H., Wetterich, S., 2016. Holocene ice-wedge polygon development in northern Yukon permafrost peatlands (Canada). *Quat. Sci. Rev.* 147, 279–297. <https://doi.org/10.1016/j.quascirev.2016.02.008>.
- Galley, R.J., Babb, D., Ogi, M., Else, B.G.T., Geifuss, N.-X., Crabeck, O., Barber, D., G., & Rysgaard, S., 2016. Replacement of multiyear sea ice and changes in the open water season duration in the Beaufort Sea since 2004. *J. Geophys. Res. Oceans* 121 (3), 1806–1823. <https://doi.org/10.1002/2015JC011583>.
- Government of the Northwest Territories, 2022. NWT Summary of Community Statistics. <https://www.statsnwt.ca/population/population-estimates/bycommunity.php>. (Accessed 31 March 2023).
- Grosse, G., Jones, B., Arp, C., 2013. Thermokarst lakes, drainage, and drained basins. In: Shroder, J., Giardino, R., Harbor, J. (Eds.), *Treatise on Geomorphology, Glacial and Periglacial Geomorphology*, vol. 8. Academic Press, San Diego, CA, pp. 325–353. <https://doi.org/10.1016/B978-0-12-374739-6.00216-5>.
- Gruber, S., 2020. Ground subsidence and heave over permafrost: hourly time series reveal interannual, seasonal and shorter-term movement caused by freezing, thawing and water movement. *Cryosphere* 14 (4), 1437–1447. <https://doi.org/10.5194/tc-14-1437-2020>.
- Hjort, J., Streletskiy, D., Doré, G., Wu, Q., Bjella, K., Luoto, M., 2022. Impacts of permafrost degradation on infrastructure. *Nat. Rev. Earth Environ.* 3 (1), 24–38. <https://doi.org/10.1038/s43017-021-00247-8>.
- Hoque, M.A., Pollard, W.H., 2016. Stability of permafrost dominated coastal cliffs in the Arctic. *Polar Sci.* 10 (1), 79–88. <https://doi.org/10.1016/j.polar.2015.10.004>.
- Irgang, A., Lantuit, H., Gordon, R., Piskor, A., Manson, G., 2019. Impacts of past and future coastal changes on the Yukon coast — threats for cultural sites, infrastructure, and travel routes. *Arct. Sci.* 5 (2), 107–126. <https://doi.org/10.1139/as-2017-0041>.
- James, T.S., Robin, C., Henton, J.A., Craymer, M., 2021. Relative sea-level projections for Canada based on the IPCC Fifth Assessment Report and the NAD83v70VG national crustal velocity model. *Geol. Surv. Can., Open File* 8764 (10.4095), 327878.
- Jones, B.M., Farquharson, L.M., Baughman, C.A., Buzard, R.M., Arp, C.D., Grosse, G., Bull, D.L., Günther, F., Nitze, I., Urban, F., Kasper, J.L., 2018. A decade of remotely sensed observations highlight complex processes linked to coastal permafrost bluff erosion in the Arctic. *Environ. Res. Lett.* 13 (11), 115001. <https://doi.org/10.1088/1748-9326/aae471>.
- Jones, M.K.W., Pollard, W.H., Jones, B.M., 2019. Rapid initialization of retrogressive thaw slumps in the Canadian high Arctic and their response to climate and terrain factors. *Environ. Res. Lett.* 14 (5), 055006. <https://doi.org/10.1088/1748-9326/ab12fd>.
- Jones, B.M., Grosse, G., Farquharson, L.M., Roy-Léveillé, P., Veremeeva, A., Kanevskiy, M.Z., Gaglioti, B.V., Breen, A.L., Parsekian, A.D., Ulrich, M., Hinkel, K.M., 2022. Lake and drained lake basin systems in lowland permafrost regions. *Nat. Rev. Earth Environ.* 3 (1), 85–98. <https://doi.org/10.1038/s43017-021-00238-9>.
- Kanevskiy, M., Shur, Y., Jorgenson, T., Brown, D.R., Moskalenko, N., Brown, J., Walker, D.A., Reynolds, M.K., Buchhorn, M., 2017. Degradation and stabilization of ice wedges: implications for assessing risk of thermokarst in northern Alaska. *Geomorphology* 297, 20–42. <https://doi.org/10.1016/j.geomorph.2017.09.001>.
- Kanevskiy, M., Shur, Y., Walker, D.A., Jorgenson, T., Reynolds, M.K., Peirce, J.L., Jones, B.M., Buchhorn, M., Matyshak, G., Bergstedt, H., Breen, A.L., 2022. The shifting mosaic of ice-wedge degradation and stabilization in response to infrastructure and climate change, Prudhoe Bay Oilfield, Alaska, USA. *Arct. Sci.* 8 (2), 498–530. <https://doi.org/10.1139/as-2021-0024>.
- Karjalainen, O., Luoto, M., Aalto, J., Etzelmüller, B., Grosse, G., Jones, B.M., Lilleøren, K.S., Hjort, J., 2020. High potential for loss of permafrost landforms in a changing climate. *Environ. Res. Lett.* 15 (10), 104065. <https://doi.org/10.1088/1748-9326/abaf5>.
- Kartozia, A., 2019. Assessment of the ice wedge polygon current state by means of UAV imagery analysis (Samoylov Island, the Lena Delta). *Remote Sens.* 11 (13), 1627. <https://doi.org/10.3390/rs11131627>.
- Kerr, D.E., 1994. Late Quaternary stratigraphy and depositional history of the Parry Peninsula-Perry River area, District of Mackenzie, Northwest Territories. In: *Geological Survey of Canada, Ottawa* (34 pp. ISBN 0-660-15411-0).
- Kerr, D.E., 1996. Late Quaternary Sea level history in the Paulatuk to Bathurst Inlet area, Northwest Territories. *Can. J. Earth Sci.* 33 (3), 389–403. <https://doi.org/10.1139/e96-029>.
- Kokelj, S.V., Jorgenson, M.T., 2013. Advances in thermokarst research. *Permafr. Periglac. Process.* 24 (2), 108–119. <https://doi.org/10.1002/ppp.1779>.
- Lantuit, H., Pollard, W.H., 2008. Fifty years of coastal erosion and retrogressive thaw slump activity on Herschel Island, southern Beaufort Sea, Yukon Territory, Canada. *Geomorphology* 95 (1–2), 84–102. <https://doi.org/10.1016/j.geomorph.2006.07.040>.
- Larsen, J.N., Schweitzer, P., Abass, K., Doloisio, N., Gartler, S., Ingeman-Nielsen, T., Ingimundarson, J.H., Jungsberg, L., Meyer, A., Rautio, A., Scheer, J., 2021. Thawing permafrost in Arctic coastal communities: a framework for studying risks from climate change. *Sustainability* 13 (5), 2651. <https://doi.org/10.3390/su13052651>.
- Li, G., Zhang, M., Pei, W., Melnikov, A., Khristoforov, I., Li, R., Yu, F., 2022. Changes in permafrost extent and active layer thickness in the Northern Hemisphere from 1969 to 2018. *Sci. Total Environ.* 804, 150182. <https://doi.org/10.1016/j.scitotenv.2021.150182>.
- Liew, M., Xiao, M., Farquharson, L., Nicolsky, D., Jensen, A., Romanovskiy, V., Peirce, J., Alessa, L., McComb, C., Zhang, X., Jones, B., 2022. Understanding effects of permafrost degradation and coastal erosion on civil infrastructure in Arctic coastal villages: a community survey and knowledge co-production. *J. Mar. Sci. Eng.* 10 (3), 422. <https://doi.org/10.3390/jmse10030422>.
- Liljedahl, A.K., Boike, J., Daanen, R.P., Fedorov, A.N., Frost, G.V., Grosse, G., Hinzman, L.D., Iijima, Y., Jorgenson, J.C., Matveyeva, N., Necsoiu, M., 2016. Pan-Arctic ice-wedge degradation in warming permafrost and its influence on tundra hydrology. *Nat. Geosci.* 9 (4), 312–318. <https://doi.org/10.1038/ngeo2674>.
- MacKay, J., 2002. Thermally induced movements in ice-wedge polygons, western arctic coast: a long-term study. *Géog. Phys. Quatern.* 54 (1), 41–68. <https://doi.org/10.7202/004846ar>.
- Mackay, J.R., Burn, C.R., 2005. A long-term field study (1951–2003) of ventifacts formed by katabatic winds at Paulatuk, western Arctic coast, Canada. *Can. J. Earth Sci.* 42 (9), 1615–1635. <https://doi.org/10.1139/e05-061>.
- McCrystall, M.R., Stroeve, J., Serreze, M., Forbes, B.C., Screen, J.A., 2021. New climate models reveal faster and larger increases in Arctic precipitation than previously projected. *Nat. Commun.* 12 (1), 6765. <https://doi.org/10.1038/s41467-021-27031-y>.
- NASA, Power Data Access. n.d. Wind data from 1985 to 2020 at Paulatuk. <https://power.larc.nasa.gov/data-access-viewer/>. [accessed the 31/03/2023].
- Nitzbon, J., Langer, M., Westermann, S., Martin, L., Aas, K., Boike, J., 2019. Pathways of ice-wedge degradation in polygonal tundra under different hydrological conditions. *Cryosphere* 13 (4), 1089–1123. <https://doi.org/10.5194/tc-13-1089-2019>.
- Nitze, I., 2023. noaaplotter (Version 0.5.6). [Computer software]. <https://doi.org/10.5281/zenodo.7753462>.
- Obu, J., Westermann, S., Barboux, C., Bartsch, A., Delaloye, R., Grosse, G., Heim, B., Hugelius, G., Irrgang, A., Käab, A.M., Kroisleitner, C., Matthes, H., Nitze, I., Pellet, C., Seifert, F.M., Strozzi, T., Wegmüller, U., Wiczorek, M., Wiesmann, A., 2021a. ESA permafrost climate change initiative (Permafrost\_cci): permafrost active layer thickness for the northern hemisphere, v3.0. In: NERC EDS Centre for Environmental Data Analysis, 28 June 2021. <https://doi.org/10.5285/67a3f8c8dc914ef99f7f08eb0d997e23>.

- Obu, J., Westermann, S., Barboux, C., Bartsch, A., Delaloye, R., Grosse, G., Heim, B., Hugelius, G., Irrgang, A., Kääh, A.M., Kroisleitner, C., Matthes, H., Nitze, I., Pellet, C., Seifert, F.M., Strozzi, T., Wegmüller, U., Wiczorek, M., Wiesmann, A., 2021b. ESA permafrost climate change initiative (Permafrost\_cci): permafrost ground temperature for the northern hemisphere, v3.0. In: NERC EDS Centre for Environmental Data Analysis, 28 June 2021. <https://doi.org/10.5285/b25d4a6174de4ac78000d034f500a268>.
- Oldenborger, G.A., LeBlanc, A.M., 2015. Geophysical characterization of permafrost terrain at Iqaluit International Airport, Nunavut. *J. Appl. Geophys.* 123, 36–49. <https://doi.org/10.1016/j.jappgeo.2015.09.016>.
- Oliva, M., Vieira, G., Pina, P., Pereira, P., Neves, M., Freitas, M.C., 2014. Sedimentological characteristics of ice-wedge polygon terrain in Adventdalen (Svalbard)—environmental and climatic implications for the late Holocene. *Solid Earth* 5 (2), 901–914. <https://doi.org/10.5194/se-5-901-2014>.
- Radosavljevic, B., Lantuit, H., Pollard, W., Overduin, P., Couture, N., Sachs, T., Helm, V., Fritz, M., 2016. Erosion and flooding—threats to coastal infrastructure in the Arctic: a case study from Herschel Island, Yukon Territory, Canada. *Estuar. Coasts* 39 (4), 900–915. <https://doi.org/10.1007/s12237-015-0046-0>.
- Raynolds, M.K., Walker, D.A., Ambrosius, K.J., Brown, J., Everett, K.R., Kanevskiy, M., Kofinas, G.P., Romanovsky, V.E., Shur, Y., Webber, P.J., 2014. Cumulative geocological effects of 62 years of infrastructure and climate change in ice-rich permafrost landscapes, Prudhoe Bay Oilfield, Alaska. *Glob. Chang. Biol.* 20 (4), 1211–1224. <https://doi.org/10.1111/gcb.12500>.
- Sankar, R., Murray, M., Wells, P., 2019. Decadal scale patterns of shoreline variability in Paulatuk, N.W.T, Canada. *Polar Geogr.* 42 (3), 196–213. <https://doi.org/10.1080/1088937x.2019.1597395>.
- Smith, S.L., Romanovsky, V.E., Lewkowicz, A.G., Burn, C.R., Allard, M., Clow, G.D., Yoshikawa, K., Throop, J., 2010. Thermal state of permafrost in North America: a contribution to the international polar year. *Permafr. Periglac. Process.* 21 (2), 117–135. <https://doi.org/10.1002/ppp.690>.
- Smith, S.L., O'Neill, H.B., Isaksen, K., Noetzli, J., Romanovsky, V.E., 2022. The changing thermal state of permafrost. *Nat. Rev. Earth Environ.* 3 (1), 10–23. <https://doi.org/10.1038/s43017-021-00240-1>.
- Tanguy, R., Whalen, D., Prates, G., Vieira, G., 2023. Shoreline change rates and land to sea sediment and soil organic carbon transfer in eastern Parry Peninsula from 1965 to 2020 (Amundsen Gulf, Canada). *Arct. Sci.* <https://doi.org/10.1139/as-2022-0028e-First>.
- Wainwright, H.M., Liljedahl, A.K., Dafflon, B., Ulrich, C., Peterson, J.E., Gusmeroli, A., Hubbard, S.S., 2017. Mapping snow depth within a tundra ecosystem using multiscale observations and Bayesian methods. *Cryosphere* 11 (2), 57–875. <https://doi.org/10.5194/tc-11-857-2017>.
- Whalen, D., Forbes, D.L., Kostylev, V., Fraser, P., Nedimovic, M.R., Stuckey, S., 2022. Mechanisms, volumetric assessment, and prognosis for rapid coastal erosion of Tuktoyaktuk Island, and important natural barrier for the harbour and community. *Can. J. Earth Sci.* 59 (11), 945–960. <https://doi.org/10.1139/cjes-2021-0101>.
- Yorath, C.J., Balkwill, H.R., Klassen, R.W., 1975. Franklin Bay and Malloch Hill Map Areas, District of Mackenzie. In: Geological Survey of Canada, Paper. <https://doi.org/10.4095/102527> (pp. 74–36).